Colloids and Surfaces B: Biointerfaces 110 (2013) 156–162

Contents lists available at SciVerse ScienceDirect

Colloids and Surfaces B: Biointerfaces

journal homepage: www.elsevier.com/locate/colsurfb

# Interfacial study of cell adhesion to liquid crystals using widefield surface plasmon resonance microscopy

Chin Fhong Soon [a,b,*], Seyed Ali Khaghani [c], Mansour Youseffi [c], Nafarizal Nayan [a], Hashim Saim [a], Stephen Britland [d], Nick Blagden [e], Morgan Clive Thomas Denyer [b]

[a] Biosensor and Bioengineering Laboratory, MiNT-SRC Research Center, Universiti Tun Hussein Onn Malaysia, 86400 Parit Raja, Batu Pahat, Johor, Malaysia
[b] School of Medical Sciences, University of Bradford, Bradford BD7 1DP, United Kingdom
[c] School of Engineering, Design and Technology-Medical Engineering, University of Bradford, Bradford BD7 1DP, United Kingdom
[d] Department of Pharmacy, School of Science and Engineering, University of Wolverhampton, City Campus - South Wulfruna St, Wolverhampton, WV1 1LY, United Kingdom
[e] Lincoln School of Pharmacy, University of Lincoln, Brayford Pool, Lincoln, Lincolnshire, LN6 7TS, United Kingdom

ARTICLE INFO

*Article history:*
Received 20 February 2013
Received in revised form 10 April 2013
Accepted 16 April 2013
Available online xxx

*Keywords:*
Widefield surface plasmon resonance microscopy
Cell adhesion
Keratinocytes
Cell–liquid crystal interface

ABSTRACT

Widefield surface plasmon resonance (WSPR) microscopy provides high resolution imaging of interfacial interactions. We report the application of the WSPR imaging system in the study of the interaction between keratinocytes and liquid crystals (LC). Imaging of fixed keratinocytes cultured on gold coated surface plasmon substrates functionalized with a thin film of liquid crystals was performed in air using a 1.45 NA objective based system. Focal adhesion of the cells adhered to glass and LC were further studied using immunofluorescence staining of the vinculin. The imaging system was also simulated with $2 \times 2$ scattering matrix to investigate the optical reflection of the resonant plasmonic wave via the glass/gold/cell and glass/gold/LC/cell layers. WSPR imaging indicated that keratinocytes are less spread and formed distinct topography of cell–liquid crystal couplings when cultured on liquid crystal coated substrates. The simulation indicates that glass/LC shifted the surface plasmon excitation angle to 75.39° as compared to glass/air interface at 44°. The WSPR microcopy reveals that the cells remodelled their topography of adhesion at different interfaces.



## 1. Introduction

A challenge to cell based biosensor development is being able to achieve effective sensing of cell responses within support media which are chemically and rheologically compatible. To this end, our previous work has examined the emerging application of liquid crystal thin films in single cell force sensing using conventional optical microcopy [5]. These liquid crystal based biosensors enable cell adhesion and contractile activity to change the organization of the liquid crystals leading to the detection of cell responses [1–5]. Our study [5] indicated that cholesteryl ester liquid crystals can support cell adhesion and allow the detection of cellular contractions without pre-coating the liquid crystals with adhesion ligands. Although cell-surface interactions have recently been examined with liquid crystals functioning as the force transducer, it is not understood how soft substrates such as liquid crystals affect the organization of the focal adhesions that enable cell attachment to a culture substrate.

Surface plasmons (SP) are highly sensitive to dielectric permittivity changes on a metal-dielectric surface [6]. Thus, surface plasmon technology has been used in the development of light microscope system in which differences in the optical densities of the imaging target alter the way p-polarized light couples into surface plasmons. This results in varying amount of light reflected from a metallic coated surface such as a gold coated glass substrate [7]. This means that surface plasmon microscopy allows the acquisition of a sample image in which contrast is dependent on the relative intensity of the reflected light, and this in turn is dependent on the macromolecular interfacial optical density. Surface Plasmon microscopes allow high contrast imaging of antigen-antibody bindings in cells [8], monitoring local impedance changes in relation to the dynamics of cellular process [9] and determining the mass of the fibronectin absorbed on glass substrate [10]. Attempts to interrogate the surface interactions of cells using surface plasmon microscope have been made, in which, the system incorporated an aluminium coated prism [11]. Although this system enabled reasonably high resolution imaging of the cell-surface interface, the microscope was limited by poor

* Corresponding author at: Biosensor and Bioengineering Laboratory, MiNT-SRC Research Center, Universiti Tun Hussein Onn Malaysia, 86400 Parit Raja, Batu Pahat, Johor, Malaysia. Tel.: +60 4538614; fax: +60 4536060.
*E-mail addresses:* fionasoon@gmail.com, soon@uthm.edu.my (C.F. Soon).

0927-7765/$ – see front matter © 2013 Elsevier B.V. All rights reserved.
http://dx.doi.org/10.1016/j.colsurfb.2013.04.012

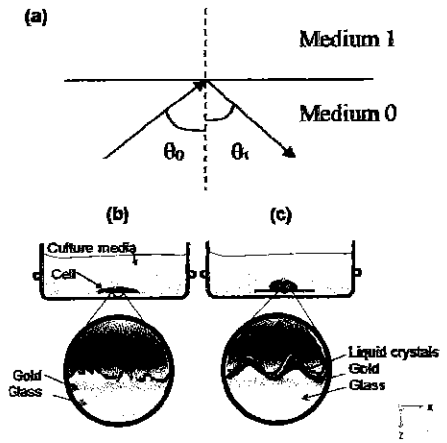


**Fig. 1.** (a) An incident light strikes interface of medium 0/1 at an angle $\theta_o$ and reflected in medium 0 at angle $\theta_1$. The graphical representations of cells culture in the (b) absence and (c) presence of liquid crystals on gold substrates.

contrast resolution of cellular structure due to the wide angles over which p-polarized light excited surface plasmons. To circumvent this optical limitation, the Widefield Surface Plasmon Microscopy (WSPR) was developed [12]. This microscope uses a high numerical aperture lens (either NA 1.45 or 1.65) and a system in which p-polarized light at a wavelength of 633 nm is applied via a rotatable diffuser before striking to gold coated substrate. The WSPR has been used to imaging of lamellipodium of human keratinocytes with good contrast at resolutions down to 500 nm [12]. To date, surface plasmon microscopy has not been used to examine cells on liquid crystals.

The novel aim in this study is the use of widefield surface plasmon microscopy to capture interfacial images of cells grown on liquid crystals in order to examine the restructuring of the adhesion plaques of cells cultured on soft substrates. In order to support the observations obtained by WSPR microscopy, immunocytochemical staining against vinculin will be used to confirm the outcomes of the WSPR study in relation to any observed changes on focal adhesion distribution. In order to understand the effects of the optical reflectivity when adding a liquid crystal layer to a glass/gold substrates interfacial substrate, Fresnel's equation will be used to determine the reflectance of light incident on a multilayer system consists of a glass/gold and glass/gold/liquid crystal system. In consideration of the multilayer reflection, a 2 × 2 scattering matrix technique will be used to solve the reflective coefficients for the multilayer system.

## 2. Materials and methods

### 2.1. Simulation of widefield surface plasmon resonance profiles

Simulation of the WSPR optical function was performed using MATLAB Integrated Development Environment software. Fresnel's equations were used to compute the reflectance of light incident on a multilayer system consisting of either a layer of liquid crystal extending beyond the evanescent field on a gold coated glass cover slip or a simple gold coated glass cover slip. Surface plasmons can be excited at the metal-dielectric interface when an incident light strikes on the interface at a specific angle. At the resonance angle, the energy carried by the photons of light is transferred to the interfacial electrons generating a surface plasmons wave. The efficiency of this coupling can be measured in a surface plasmon microscope by measuring the light reflected by a gold coated surface.

Consider a ray of incident light striking at the interface between medium 0 and 1 (Fig. 1a). Each has a refractive index of $N_0$ and $N_1$ respectively. The incident wave vector with amplitude of $E_0$ arrived to the interface at an angle of $\theta_o$ with respect to the normal plane.

The Fresnel's coefficients of the reflectance of the s-polarized and p-polarized light are given by

$$r_{01S} = \left|\frac{E_0^-}{E_0^+}\right| = \frac{N_0 \cos\theta_0 - N_1 \cos\theta_1}{N_0 \cos\theta_0 + N_1 \cos\theta_1} \tag{1}$$

$$r_{01P} = \left|\frac{E_0^-}{E_0^+}\right| = \frac{N_1 \cos\theta_0 - N_0 \cos\theta_1}{N_1 \cos\theta_0 + N_0 \cos\theta_1} \tag{2}$$

where $r_{01s}$ and $r_{01p}$ are the reflection coefficients for s-polarized and p-polarized light, respectively. $\theta_o$ and $\theta_1$ are the angles of incident and refraction, respectively as obtained from Snell's law [13].

The method for computing the reflectance of the glass/gold/air and glass/gold/LC systems (Fig. 1a) is based on the application of 2 × 2 scattering matrix [14]. The equation can be expressed as the product of the interface matrices, $I$ and the layer matrices, $L$. It describes the effects of light interaction with individual interfaces and layers of the entire stratified structures as

$$\begin{vmatrix} E_0^+ \\ E_0^- \end{vmatrix} = \begin{bmatrix} S_{11} & S_{12} \\ S_{21} & S_{22} \end{bmatrix} \begin{bmatrix} E_n^+ \\ 0 \end{bmatrix} \tag{3}$$

From Eq. (3), we obtained

$$E_0^+ = S_{11} E_n^+ \tag{4}$$

and

$$E_0^- = S_{21} E_n^+ \tag{5}$$

Therefore,

$$r = \frac{E_0^-}{E_0^+} = \frac{S_{21}}{S_{11}} \tag{6}$$

$$t = \frac{1}{S_{11}} \tag{7}$$

The matrix S for a three layers system (1, 2 and 3) is

$$S = I_0 L_1 I_{12} L_2 I_{23} L_3 \tag{8}$$

The matrix I of an interface between two medium a and b is given by

$$I_{ab} = \frac{1}{t_{ab}} \begin{bmatrix} 1 & r_{ab} \\ r_{ab} & 1 \end{bmatrix} \tag{9}$$

where the layer matrix for layer $L_b$ is given by

$$L_b = \begin{bmatrix} e^{i\beta} & 0 \\ 0 & e^{i\beta} \end{bmatrix} \tag{10}$$

where $\beta$ is the phase shift that is dependent on the layer thickness ($d_b$), index of refraction ($N_b$) and angle of refraction ($\theta_b$), therefore,

$$\beta = K N_b d_b \cos\theta_b \tag{11}$$

and

$$K = \frac{2\pi}{\lambda} \tag{12}$$

where $K$ is the wavevector and $\lambda$ is the wavelength of incident light.

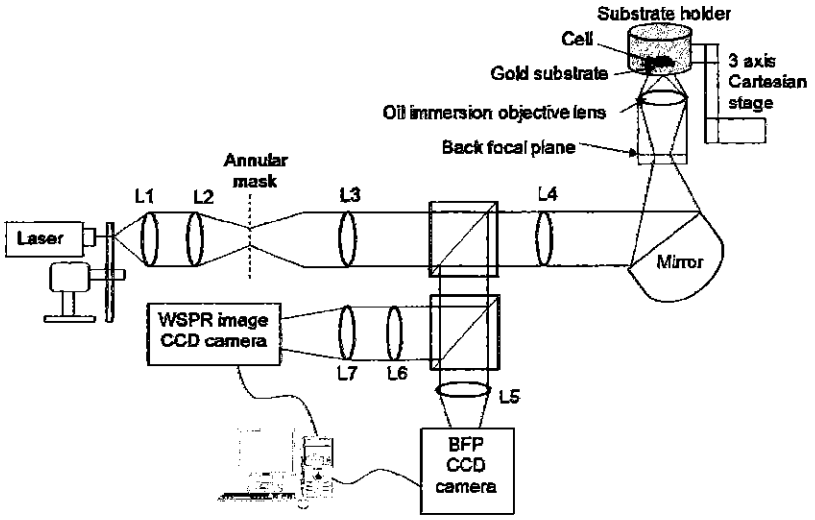


**Fig. 2.** The configuration of a widefield surface plasmon resonance microscopy system.

By determining $S$ for the multilayer system, the total reflectance is given by

$$R = \left[\frac{E_0^-}{E_0^+}\right]^2 = \left[\frac{S_{21}}{S_{11}}\right]^2 \quad (13)$$

Gold has a complex refractive index of $-12.3 + j1.29$ [15] at $\lambda = 632.8$ nm while the refractive index for glass, liquid crystal and air are 1.515, 1.558 and 1.0003, respectively [16–20]. The thickness of gold and liquid crystals after immersion in cell culture media are 50 and 5000 nm, respectively. The oil immersion objective used has a refractive index of 1.512. Cholesteryl ester liquid crystal is an anisotropic material that may have more than one reflective indices [21]. However, in monochromatic imaging of the WSPR, only the mean refractive index of the liquid crystal was considered for this material [16,18,20].

### 2.2. Cell culture and preparation of imaging sample

Cells for all experiments were obtained from sub-cultured human keratinocytes cell lines (HaCaTs) that were incubated at 37 °C. Upon reaching confluency, the cells were split and re-suspended in Rosewell Park Memorial Institute media (RPMI-1640, Sigma–Aldrich, UK). Two round glass cover slips with a diameter of 22 mm and coated with a 45 nm thick gold layer were used in this study. Cholesteryl ester liquid crystals were spin-coated at 1600 rpm to a thickness of 5 μm on a gold substrate and the substrate was immersed in the 5 ml of RPMI-1640 culture medium prior to cell plating. The preparation of cholesteryl ester liquid crystals used is as described in our previous work [4]. Cells at a density of $1.0 \times 10^4$ cells/cm$^2$ were plated in the two Petri dishes, each containing one gold coated cover slip coated with or without liquid crystals (Fig. 1b, c). Subsequently, the two Petri dishes were incubated at 37 °C for 24 h. After incubation, the cells were washed in HBSS twice and fixed in 1% Formaldehyde for 6 min. Fixation was followed by a 5 min wash and dehydration by a series of 5 min washes in serial dilutions of ethanol in distilled water from 10% through to 100% ethanol. After dehydration, each gold cover slip was transferred to a custom built WSPR microscope to be imaged (Fig. 2).

#### 2.2.1. Widefield surface plasmon resonance imaging of cell–liquid crystal interface

The WSPR microscope configuration used in the experiment is as shown in Fig. 2. A monochromatic laser diode (wavelength 633 nm) illuminated the substrate via a rotatable diffuser an annular mask and a Zeiss Plan Fluar 100× objective with a numerical aperture of 1.45 coupled to the sample via immersion oil with a refractive index of 1.512. The rotatable diffuser allowed the sample to be illuminated with a speckled pattern when stationary, but on rotation allowed the speckled illumination to be averaged. From the diffuser, the incident light passed through a beam expander lens (L1 and L2) before striking the annular mask. The annular mask was coupled to the back focal plan (BFP) allowing the angle of incidence on the substrate via the objective lens to be optimized, whilst blocking out unwanted light. Light reflected from the sample was then directed via a beam splitter to an imaging arm and an arm enabling the imaging of the BFP. In our experiments, the incident p-polarized light from the laser diode was used to excite surface plasmons at the gold layer at an excitation angle ($\theta_p$) of 44°. The system enabled imaging of the back focal plane and the sample via two separate charge-coupled devices (CCD) cameras linked to Scion software on a personal computer. Both images contained information associating with the interfacial interactions between cells and the surface. The interfacial interaction images acquired from the WSPR imaging system were used for the analysis of morphology changes. The projected surface area of cells (A) in the WSPR micrographs can be used to compute the index of spreading or shape index which is defined as

$$\text{Shape\_index} = \frac{4\pi A}{P^2}$$

where $A$ is the area and $P$ is the perimeter of the cell, respectively [22]. The shape index of 1 indicates a perfect circle, whereas 0 is the index for a line. Measurements of the cell projected area and perimeter were performed in ImageJ software. All values were expressed in mean ± SD.

### 2.3. Immunocytochemical staining of vinculin and nucleus

The fluorescence staining experiments were conducted to identify the expressions of vinculin for cells interacted with the cholesteryl ester liquid crystals. First, glass cover slips were coated with liquid crystals as described in Soon et al. [23]. Then, HaCaT cell cultures were prepared based on the standard cell culture

procedures as described in Soon et al. [4]. Cells were maintained under two conditions, on plain glass cover slips and on glass cover slips coated with liquid crystals, both at a density of $1.3 \times 10^3$ cells/cm$^2$. After the cells reached sub-confluency, the glass cover slips were removed from the Petri dishes and washed twice with Hanks Balanced Salt Solution (HBSS, Sigma–Aldrich, UK). Subsequently, the cells were fixed with 1% formaldehyde in HBSS for 6 min, rinsed twice with HBSS and permeabilized with 0.1% Triton X-100 for 3 min. In the staining procedure, cells were rinsed and treated with a blocking solution. For vinculin staining, the cells were bathed in HBSS containing 2% bovine serum albumin (BSA, Sigma–Aldrich, UK). After blocking, cells were washed three times in HBSS and incubated in 50 μl of monoclonal anti-human vinculin antibody (1:40 in 1% BSA, Sigma–Aldrich, UK) for 24 h in a humidity chamber at 5 °C. After incubation for 24 h, the substrates were washed three times with HBSS, blotted and incubated with goat anti-mouse Immunoglobulin (IgG) secondary antibody labelled with Alexor Fluor 488 (5 μg/ml diluted in 1% BSA, Sigma Aldrich, UK) for 1 h. After staining, the substrates were subjected to three 5 min washes in HBSS before mounting onto the glass slides with DAPI dihydrochloride (0.1 μg/ml diluted in HBSS). All the immunofluorescence staining were observed using a plan fluor lens (N.A of 1.3) Nikon Eclipse 80i fluorescence microscope under dark field (DF) at 40x magnification and the images were captured with ACT-2u software.

### 2.4. Statistical analysis

The differences between the cell projected area, cell perimeter and shape index of cells adhered to the glass and LC in three repeats of experiment were analyzed for significant differences ($N$=200, $P$<0.05) using independent $t$-test in statistical tools for social sciences (SPSS).

## 3. Results and discussion

In order to develop a robust simulation, the interface between the cells, gold substrate and LC was characterized by multiple layered optical densities. This computer simulation is needed in order to determine the feasibility of using the WSPR microscope to image a biomaterial such as a liquid crystal layered on top of a gold coated substrate. The Fresnel's equation based computer simulation was thus used to model the reflectivity in this multilayer system. However, it was modified into a $2 \times 2$ scattering matrix because this is more suitable for solving the reflectance and transmittance coefficients in a multilayer sandwich system [24]. It was assumed that LC is closely coupled to the glass without gaps. Fig. 3(a) shows the intensity of reflectance for P-polarized light ($R_p$) and for S-polarized light ($R_s$) as a function of the incident angle for the glass/gold/air system. The intensity of the reflectance for the glass/gold/air interface shows a sharp dip at 43.65° indicating the coupling of the p-polarized light into surface plasmons. This simulated angle is very close to the experimental excitation angle (44°) which was determined by scanning wide incident angles stepwise through the system and the corresponding back focal plane is as shown in Fig. 4a. Fig. 4a shows a pair of clearly defined vertical arcs formed in the back focal plane which indicates the generation of strong surface plasmons. These arcs also correspond to the dip in p-polarization reflection coefficient for the glass/gold/air interface (Fig. 3a). The strength of the dip in the vertical direction is strong compared with the dip in the horizontal direction (Fig. 4(a)). In the horizontal direction, the incident light is mainly s-polarized. For the s-polarized light, the reflectivity is rather monotonical because it does not interact with the metal-dielectric to generate evanescent waves (Fig. 3(a, b)). However, for the p-polarized light, a dip

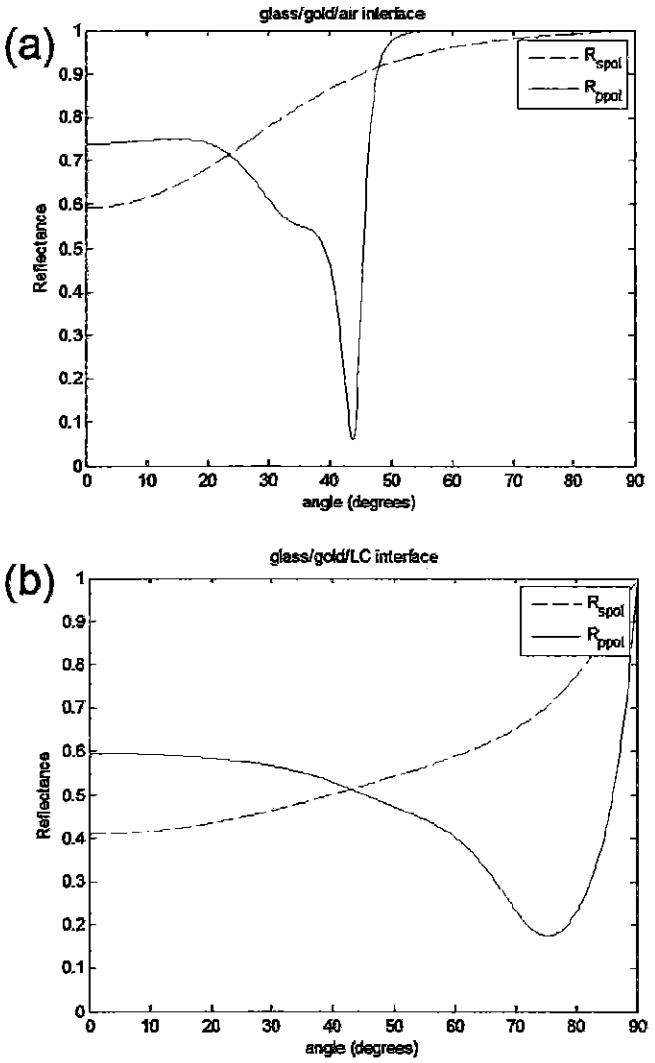


**Fig. 3.** The reflectance coefficients of the s-polarized ($R_{spol}$) and p-polarized ($R_{ppol}$) light incident at the (a) glass/gold/air and (b) glass/gold/LC systems.

at a surface plasmon excitation angle of 75.39° was found (Fig. 3b). LC with a refractive index of 1.558 nearly shifted the angle out of the range of the objective lens and this can be seen from both the reflective coefficient derived from the theoretical simulation and the experimental imaging of the back focal plane (Fig. 3 (b) and Fig. 4(b), respectively).

The sharp decrease in the reflective coefficient for the p-polarized light relates to the energy of the surface plasmons being dissipated in the gold layer. The interaction of the surface plasmons and the metallic layer generates an evanescent field at the interface between the metal and the final dielectric material (gold/LC/cell or gold/cell). The additional dielectric material (LC) deposited on the gold layer interferes with the evanescent field resulting in changes in the ability of the system to excite surface plasmons. This potentially makes the WSPR a good tool for examining deformation in a liquid crystal gel at its interface with a gold layer, in that any changes in the refractive index of the LC at the LC/gold interface will modify the ability of P-polarized light to couple into surface plasmons. The liquid crystal deformation or patterns of concentric bands observed in Fig. 5a and b arise as a result of the pressure exerted by cells via the focal adhesions in the $x$, $y$ and $z$-directions (Fig. 1b, c).

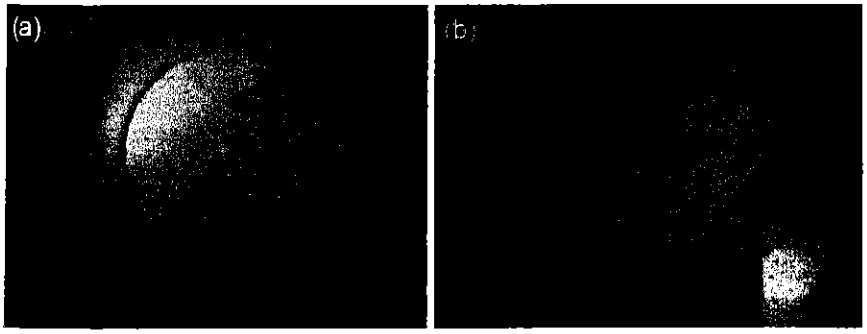


**Fig. 4.** Back focal plane of the (a) glass/gold/cell and (b) glass/gold/LC/cell systems. The inset in (b) shows the border of the contrast enhanced back focal plane for (b).

Cholesteric liquid crystals are known as the chiral nematic liquid crystals because they consist of layers of nematic molecules twisted along a helical axis at a pitch length of ~5000 nm [25,26]. The height of the evanescent field generated via a gold layer ranges from 70 to 300 nm [11,27]. At this range, one can imagine that the evanescent wave interacts with a few hundreds of the chiral nematic liquid crystal molecules (thickness of a layer = 20–35 Å) [28,29] vertically coupled to the metallic surface. Due to the anisotropic properties of the LC, the wave can be refracted by the gold/LC interface and thus could reduce much of reflective coefficient as indicated by

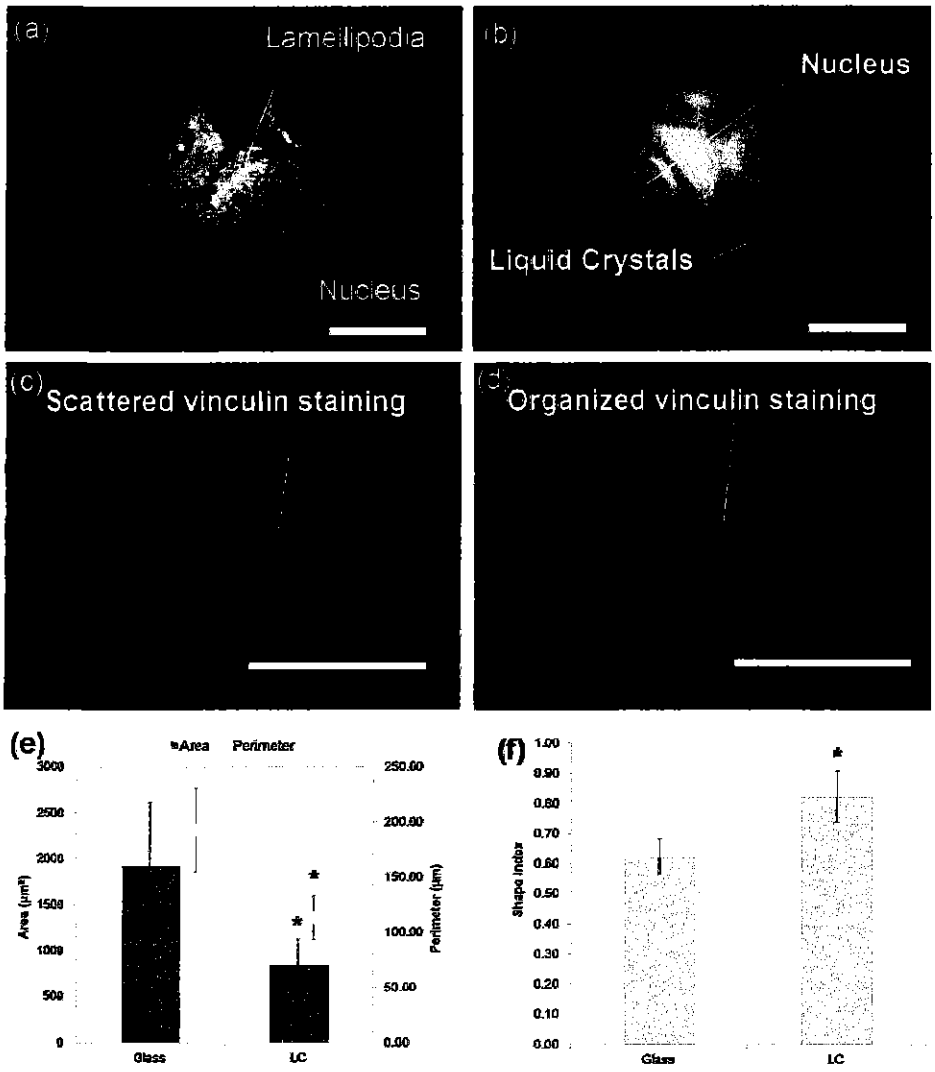


**Fig. 5.** Micrographs of WSPR imaging, staining against vinculin (green) and nucleus (blue) of the HaCaTs cultured on (a, c) hard glass cover slip and (b, d) soft liquid crystals. (e) The bar charts of area and perimeter for cells cultured on glass and liquid crystals. (f) The bar charts of shape index for cells cultured on glass and liquid crystals. The asterisks indicate that the area, perimeter and shape index for cells cultured on the glass and liquid crystals are significantly different (significant for $p < 0.05$, $t$-test, $N = 200$) (scale bar: 25 μm). (For interpretation of the references to color in this figure legend, the reader is referred to the web version of the article.)

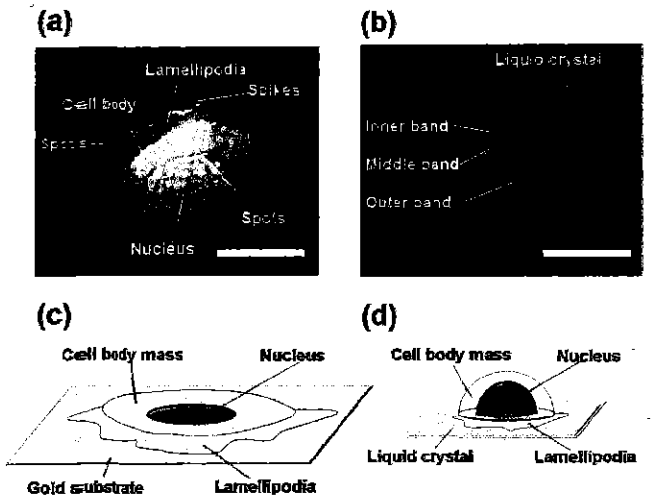


**Fig. 6.** Micrographs of WSPR imaging for single cells cultured on (a) glass and (b) liquid crystal and their corresponding graphical depictions of cell attachments on the gold and liquid crystal substrates in (c) and (d), respectively (scale bar: 25 μm).

the fading of the vertical arc in the BFP (Fig. 4b). This signifies a decrease in the surface plasmon generation in the gold/LC system. The liquid crystal phase is recognized as the fourth phase of matter with physical properties that lies in between an amorphous liquid and a solid crystal [30]. Therefore, it has the ability not just to refract incident light like a fluid but also to reflect light back to the image capturing system [20]. Despite the weakened excitation of surface plasmons, imaging the fixed cell/LC adhesion in air is still achievable (Figs. 5b, 6b) at an excitation angle of 75.39°. In the usual liquid crystal display system, light propagates perpendicular to the optical axis. The periodicity of the cholesteric phase causes a diffraction of the polarized light following the helically twisted molecules. The refractivity of the incident light from the helical structure of the cholesteric phase is difficult to be calculated but it is assumed in index of approximately 1.558 [16,18,20].

From the monochromatic micrographs generated in the WSPR system (Figs. 5a and 6a), HaCaTs cultured directly on the gold substrate (hard surface) formed a wide band like contact area with irregular spread of punctuated patterns. The wide bands represented the cell body and the centrally located nucleus (Fig. 6a, c). The close coupling of the cell to the glass surface is an indication of the large contact area at the gold/cell substrate interface. In addition, WSPR imaging reveals a thin film of lamellipodia characterized by a translucent structure (Fig. 6a). The punctuated white spots of contact appearing at the edges of the lamellipodia and the irregularly spread of regions at the cell body-gold substrate interface (Figs. 5a and 6a) are in agreement with observation of the scattered focal adhesions seen in cells spread on glass substrate (Fig. 5c). The centre band found in Fig. 5a is probably associated with the adhesion sites close to the supporting nucleus region of the cell which is also indicated in the micrograph of the DAPI (blue) stainings (Fig. 5c).

Contrarily, the cells cultured on liquid crystals (soft surface) were found to be less well spread and three clearly defined narrow concentric rings or bands in a restricted area were observed around the nucleus and the periphery of the cell (Figs. 5b and 6b). The three bands (inner, middle and outer bands) correspond to the LC couplings from the nucleus, cell body mass and small area of lamellipodia seen in cells grown on soft substrates (Fig. 6b, d). They represent topographic features associated with the cells coupling with the liquid crystal. From the WSPR micrograph (Fig. 6b), the inner band is indicative of the stress from the mass of the nucleus and this is supported by the DAPI stainings (Fig. 5d). The middle band of LC coupling was associated with the cell body mass (Fig. 6b). The outer band of LC coupling (Fig. 6b) was formed by the exertion of uniformly arranged short focal adhesions (Fig. 5d). This gave an indication that the stresses of the focal adhesions were reasonably regular around the periphery of the cell membrane when cells were coupled by liquid crystals to the gold substrate. The grey and dark areas in between the bands indicate weak adhesion and no adhesion, respectively. Immunofluorescence staining of α and β integrins in cells cultured on plain and liquid crystal coated substrates only showed the general distribution of the integrins on the cell surface (unpublished result), whilst the vinculin staining reported here was useful in supporting the view that the interfacial structures observed in WSPR imaging were associated with focal contact formation. However, it was apparent that conventional immunocytochemical imaging did not allow the identification of the thin lamellipodia and the topographic features associated with cell-surface interactions caused by the cell body mass observed via the WSPR microscope in cells cultured on plain WSPR substrates and LC coated WSPR substrates

As shown in Fig. 5e, the projected area ($2400.70 \pm 856.26\ \mu m^2$) of cell on the glass is significantly larger ($N = 200$, $p = 0.05$) than those cells cultured on the liquid crystal substrate ($849.36 \pm 277.26\ \mu m^2$). The perimeter of the cells adhered to the glass slides ($192.93 \pm 37.59\ \mu m$) is also larger than ($N = 200$, $p = 0.05$) the cells spread on LC substrates ($112.99 \pm 19.81\ \mu m$). The shape index in Fig. 5f indicates that the cells cultured on the LC substrates had taken round morphology (shape index $= 0.82 \pm 0.08$) whereas cells spread in poly-hedral shapes on the glass substrates (shape index $= 0.62 \pm 0.06$). The shape indices are significantly different for $p = 0.09$. These results indicate that the softness of the culture substrate plays a role of the mechanical signal in regulating the interface topology and indicates a change in the phenotype of the cell [31]. Clearly, the dynamic behaviour of cells in accommodating to the stiffness of the liquid crystal substrate has induced significantly smaller vinculin staining regions that applied regular stresses at the edges of the cell membrane [32]. This supports the idea that cells have a closed-loop mechano-sensing mechanism that constantly sense the stiffness of the surrounding substrate, and changes in this stiffness can subsequently result in remodelling of the cytoskeleton and reorganization of focal adhesions.

Although surface plasmon resonance microscopy has been applied in experiments to acquire images of the cell surface features, it has not been used to image cell cultured on a thin film such as liquid crystals capable of bio-sensing [1,3,33]. A recent study [5] suggested that liquid crystals may be used as a transducer in detecting cell traction forces. However, such a liquid crystal based cell traction force measurement is limited by the resolution of the imaging systems in the *xy*-direction. It is possible that the resolution of this system may be enhanced by a WSPR system being used to image cell induced deformations in the liquid crystals towards the vertical direction (*z*-direction). The evidence presented in this paper certainly suggests that this may be the case and that a liquid crystal coated surface plasmon system may be used to interrogate the stresses generated between a cell and a soft substrate enabling further interrogation of the influence of cell signalling systems on the forces exerted on a substrate by cells. Although the WSPR system can be used to map the interfacial stresses associated with cell surface adhesions, the system isn't optimized. To image using a surface plasmon system, one has to ensure that the biomaterial placed on the gold substrate has an optical density (refractive index) close to the refractive index of the glass/gold substrate. It is probable that if live cells grown on LC coated WSPR substrates were imaged in culture media, the culture media would provide a refractive index close to that of water $n \sim 1.33$ in the system [17]. This tends to shift the excitation angle of surface plasmon out of the objective lens and subsequently, impede the surface plasmon activity leading to

retardation in the imaging as experienced in our experiment. This specific problem can be resolved by using a higher NA oil immersion lens in the WSPR system as reported in Somekh et al. [7] but the spatial resolution in this case needs further enhancements.

## 4. Conclusion

In this work, the WSPR microscope was found to be an effective tool in interrogating cell-soft surface interactions. The organization of focal adhesions and location of the nucleus found in immunofluorescence stainings matched the observations in the WSPR imaging except in details associated with the coupling between the cell body mass and the surface. WSPR imaging revealed that cell body mass could contribute to different topographic features at the cell-surface interface depending on the absence and presence of a soft substrate such as a thin liquid crystal film. Results to date also indicated that cell growth on soft substrates resulted in a reduced cell adhesion area and was associated with the remodelling of focal adhesions. Through the simulation of the reflective coefficients of the s-polarized and p-polarized, the parameters showed a decrease in the surface plasmon excitation when liquid crystals were used as coupling medium. Theoretical simulation suggested that liquid crystals could shift the excitation angle to a higher order yet provide sufficient reflectivity to allow surface plasmon resonance imaging.

## Acknowledgments

The authors would like to acknowledge Professor Des Tobin, Dr. Rebecca Berends and Dr. Samira Batista Lobo for providing technical advices and support. We thank Malaysia Ministry of Higher Education for providing research funding support (FRGS Grant Vot No. 1050).

## References

[1] J.J. Hwang, S.N. Iyer, L.S. Li, R. Claussen, D.A. Harrington, S.I. Stupp, Self-assembling biomaterials: liquid crystal phases of cholesteryl oligo(L-lactic acid) and their interactions with cells, Proc. Natl. Acad. Sci. U. S. A. 99 (2002) 9662–9667.
[2] J. Fang, W. Ma, J.V. Selinger, R. Shashidhar, Imaging biological cells using liquid crystals, Langmuir 19 (2003) 2865–2869.
[3] N. Lockwood, J.C. Mohr, L. Ji, C.J. Murphy, S.P. Palecek, J.J. d. Pablo, N.L. Abbott, Thermotropic liquid crystals as substrates for imaging the reorganization of matrigel by human embryonic stem cells, Adv. Funct. Mater. 16 (2006) 618–624.
[4] C.F. Soon, M. Youseffi, T. Gough, N. Blagdenand, M.C.T. Denyer, Rheological characterization of the time-dependent cholesteric based liquid crystals and in-situ verification, Mater. Sci. Eng. C 31 (2011) 1389–1397.
[5] C.F. Soon, M. Youseffi, R.F. Berends, N. Blagdenand, M.C.T. Denyer, Development of a novel liquid crystal based cell traction force transducer system, Biosens. Bioelectron. 39 (2013) 14–20.
[6] A. Otto, Excitation of nonradiative surface plasma waves in silver by the method of frustrated total reflection, ZeitschriftfürPhysik A: Hadrons Nuclei 216 (1968) 398–410.
[7] M.G. Somekh, Surface plasmon fluorescence microscopy: an analysis, J. Microsc. 206 (2002) 120–131.
[8] Y. Yanase, A. Araki, H. Suzuki, T. Tsutsui, T. Kimura, K. Okamoto, T. Nakatani, T. Hiragun, M. Hide, Biosensors, Bioelectronics 25 (2010) 1244–1247.
[9] W. Wang, K. Foley, X. Shan, S. Wang, S. Eaton, V.J. Nagaraj, P. Wiktor, U. Patel, N. Tao, Single cells and intracelluar processes studied by a plasmonic-based electrochemical impedance microscopy, Nature Chem. 3 (2011) 249–255.
[10] A.W. Peterson, M. Halter, A. Tona, K. Bhadriraju, A.L. Plant, Surface plasmon resonance imaging of cells and surface-associated fibronectin, BMC Cell Biol. 10 (2009) 1471–2121.
[11] K.-F. Giebel, C. Bechinger, S. Herminghaus, M. Riedel, P. Leiderer, U. Weiland, M. Bastmeyer, Imaging of cell/substrate contacts of living cells with surface plasmon resonance microscopy, Biophys. J. 76 (1999) 509–516.
[12] M.M.A. Jamil, M.C.T. Denyer, M. Youseffi, S.T. Britland, S. Liu, C.W. See, M.G. Somekhand, J. Zhang, Imaging of the cell surface interface using objective coupled widefield surface plasmon microscopy, J. Struct. Biol. 164 (2008) 75–80.
[13] M. Born, E. Wolf, Principles of Optics: Electromagnetic Theory of Propagation, Interference and Diffraction of Light, 9th ed., Cambridge University Press, Cambridge, 1999.
[14] R.M.A. Azzam, N.M. Bashara, Ellipsometry and Polarized Light, Elservier North Holland, Netherlands, 1996.
[15] L.G. Schulz, F.R. Tangherlini, Optical constants of silver, gold, copper, and aluminum. II. The index of refraction n, J. Opt. Soc. Am. 44 (1954) 362–367.
[16] R. Manohar, J.P. Shukla, Refractive indices, order parameter and principal polarizability of cholesteric liquid crystals and their homogeneous mixtures, J. Phys. Chem. Solids 65 (2004) 1643–1650.
[17] M.G. Somekh, Surface plasmon and surface wave microscopy, in: Optical Imaging and Microscopy, Springer, Berlin/Heidelberg, 2007 (Chapter 10).
[18] Y. Hata, J. Hoer, W. Insull, Cholesteryl ester-rich inclusions from human aortic fatty streak and fibrous plaque lesions of atherosclerosis, Am. J. Pathol. 75 (1974) 423–456.
[19] L. Novotny, B. Hecht, Surface Plasmon, Cambridge University Press, Cambridge, 2006 (Chapter 12).
[20] N.M. Chao, K.C. Chu, Y.R. Shen, Local refractive index measurement on a cholesteric liquid crystal using the surface plasmon technique, Mol. Cryst. Liq. Cryst. 67 (1981) 261–275.
[21] P.J. Collings, Liquid crystals: Nature's Delicate Phase of Matter, Princeton University Press, New Jersey, 2002.
[22] B.O. Palssonand, S.N. Bahatia, Tissue Engineering, Pearson Prentice Hall, New Jersey, 2004.
[23] C.F. Soon, M. Youseffi, N. Blagden, R. Berends, S.B. Lobo, F.A. Javid and M. Denyer, Interactions of cells with elastic cholesteryl liquid crystals Proc. IFBME, 25/X (2009) 9–12.
[24] M.A. Siddig, Z.A. Hassan, H. Zainuddin, W.M. Mat Yunus, Modeling of the optical functions for mutilayer thin film, Suranaree J. Sci. Technol. 10 (2003) 40–46.
[25] N.V. Madhusudana, Recent advances in thermotropic liquid crystals, Curr. Sci. 80 (2001) 1018–1025.
[26] G. Chilaya, Cholesteric liquid crystals: optics electro-optics and photo optics, in: H.S.K.C. Bahr (Ed.), Chirality in Liquid Crystals, Springer, New York, 2001.
[27] H. Kano, W. Knoll, A scanning microscope employing localized surface-plasmon-polaritons as a sensing probe, Opt. Commun. 182 (2000) 11–15.
[28] S.S. Katz, G.G. Shipley, D.M. Small, Physical chemistry of the lipids of human atherosclerotic lesions, Clin. Investig. 58 (1976) 200–211.
[29] E.B. Priestley, P.J. Wojtowiczand, P. Sheng, Introduction to Liquid Crystals, Plenum Press, New York and London, 1974, pp. 3.
[30] P.G. Gennes, The Physics of Liquid Crystals, The International Series of Monographs on Physics, Clarendon Press, Oxford, 1974, pp. 6.
[31] D.E. Discher, P. Janmeyand, Y.-l. Wang, Tissue cells feel and respond to the stiffness of their substrate, Science 310 (2005) 1139–1143.
[32] C.F. Soon, M. Youseffi, N. Blagden, M. Denyer, Investigation of cell adhesion, contraction and physical restructuring on shear sensitive liquid crystals, in: S. L. Ao, L. Gelman (Ed.), Electrical Engineering and Applied Computing, vol. 90, Springer, London, 2011, pp. 622–636.
[33] C.F. Soon, M. Youseffi, N. Blagden, M. Denyer, Measurement and mapping of cell traction forces on liquid crystal based force transducer, in: J.F. Whidborne, P. Willis, G. Montana (Eds.), International Conference on Computational Biosciences, vol. 742, Computational Bioscience Acta Press, Cambridge University, 2011.